

ATTITUDE AND ANGULAR RATE ESTIMATION FROM VECTOR MEASUREMENTS OF MAGNETOMETER AND SUN SENSOR FOR A LOW-COST SATELLITE

Davi Antônio dos Santos, davists@ita.br

Jacques Waldmann, jacques@ita.br

Instituto Tecnológico de Aeronáutica – Department of Systems and Control – 12228-900 – São José dos Campos, SP, Brazil

Abstract. *An autonomous attitude determination system (SDA) is proposed for a low-budget, low-earth orbit, spin-stabilized satellite with onboard magnetometer and sun sensors. The satellite can be injected into orbit either with a high spin or 3-axis controlled. The attitude control system (ACS) should act to point the satellite spin axis orthogonal to the direction of the Sun without incurring into violations of the thermal safety constraints during acquisition of the desired spin-axis pointing and spin rate previous to the onset of the operational phase. The SDA is a component of a closed-loop, 3-axis ACS with purely magnetic, magnetotorquers-only, actuation based on attitude and angular velocity estimates from vector measurements of the Sun direction and geomagnetic field. Extended Kalman and unscented estimators are tested against synthetic sensor data. The results indicate that the sensor suite and estimation algorithms intended for use onboard ITASAT provide diverging attitude estimates during the initial slow angular motion – which occurs after separation from a 3-axis-controlled launcher's last stage - when the satellite undergoes the approximately 35-minute eclipse interval that occurs in each of the desired 100-minute period, 750km-altitude, 25°-inclination target orbit. Thus, closed-loop control during eclipse intervals should be weighted carefully against thermal safety constraints on ITASAT's attitude relative to the Sun. Consequently, magnetotorquer-only control for desired attitude and spin rate acquisition should not engage during the eclipse intervals, thus lengthening the time needed since satellite injection up to the onset of the operational phase and battery recharging. This investigation yielded results useful for the undergoing effort to cope with the available sensor suite and actuators, mission analysis, and the various tradeoffs involved in developing ITASAT – a Brazilian university satellite – mostly designed in ITA under the auspices of the Brazilian Space Agency (AEB) and the Brazilian Institute for Space Research (INPE).*

Keywords: *satellite; attitude; estimation; unscented filter; extended Kalman filter.*

1. INTRODUCTION

Instances of the present trend towards small-sized, light-weight, and low-cost satellites are the various university satellites, such as AAU CUBESAT (Krogh, 2002), NCUBE (Svartveit, 2003) and Orsted (Bak *et al.*, 1996). Usual sensors for attitude determination onboard such satellites are the magnetometers and Sun sensors. Though rate-gyros are not usually found in the sensor suite in low-cost university satellites, information about the satellite angular rate is often called for in 3-axis attitude control and to propagate the attitude estimates. Hence, angular rate estimates are required from data provided by the available onboard, low-cost, attitude sensors providing vector measurements (Challa *et al.*, 1996) to control attitude with purely magnetic actuation by means of magnetotorquers that interact with the geomagnetic field (Shigehara, 1972; Bak *et al.*, 1996).

The following describes ongoing research and development of the attitude determination system for ITASAT (Figure 1) based on three two-axis Sun sensors (SS₁, SS₂ e SS₃) and a three-axis magnetometer (SM). First phase in the mission is to acquire the correct attitude and spin rate for spin stabilization after separation from the launch vehicle. Presently, it is unknown whether the launch vehicle will inject the satellite into orbit in a tumbling motion demanding 3-axis control, or already spinning at a very high angular rate – thus, the devised control system should consider both conditions. After this first phase intended for correct attitude and spin rate acquisition, the second phase is spin-stabilized as ITASAT should relay data from meteorological stations distributed over the Brazilian territory to a data-collecting station. A third, experimental phase is under consideration, in which ITASAT would function as a pointing testbed for gauging the accuracy of the 3-axis attitude control law based on the low-accuracy data from its sensor suite.

The desired attitude is constrained to maintain the spin axis pointing along the direction of highest inertia, and concurrently orthogonal with respect to the direction of the Sun to comply with the thermal safety of onboard equipment. ITASAT is expected to present a mass of 73.6kg, sized 700mmx700mmx650mm, and its desired orbit is, presently, circular, with an altitude of 750 km and 25 degrees of inclination.

As an innovation, ITASAT does require 3D angular rate estimation for closed-loop control and attenuation of the nutation angle by purely magnetic actuation and does not resort to a nutation ring partially filled with silicone oil as occurred in the design of the previous SCD-1 and 2 satellite attitude control laws (Lopes *et al.*, 1986). At that time, the launch vehicle was known to insert both SCD satellites already spinning at the target orbit and in the vicinity of the desired attitude. This is not known for a fact in the present ITASAT's mission analysis status, as its low-cost budget assumes launching shall occur in a piggyback arrangement under a primary payload. Hence, ITASAT's low-cost, crude-accuracy attitude control system (ACS) has been devised to operate on a rigid-body configuration that prevents sloshing

when attenuating the tumbling motion that is likely to come about in the case of separation from a 3-axis stabilized launcher, and yet provide the capability of acquiring the desired attitude and spin rate from a wide range of initial conditions.

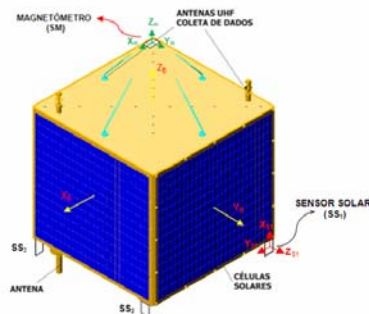


Figura 1. ITASAT's present configuration and available sensor suite.

2. ATTITUDE AND ANGULAR RATE ESTIMATION WITH VECTOR MEASUREMENTS

The minimum-variance (MV) approach to attitude estimation with vector measurements is briefly described (Wahba, 1965). S_b is a coordinate frame attached to the satellite body, aligned with the principal axes, and S_r is a reference coordinate frame, here considered to be aligned with the Earth Centered Inertial Frame. S_b rotates at time t with the angular rate vector $\omega(t) \in \mathfrak{R}^3$ with respect to S_r . A set of m vector measurements at time t is represented in S_b as the set $B(t) = \{b_i(t) \in \mathfrak{R}^3, i = 1, 2, \dots, m\}$, and in S_r as the corresponding set $R(t) = \{r_i(t) \in \mathfrak{R}^3, i = 1, 2, \dots, m\}$. The goal is to find a minimum-variance estimate of vector $p(t) \in \mathfrak{R}^3$ such that $D(p(t))$ is the direction cosine matrix (DCM) that transforms the vector representation in S_r to that in S_b . The components of $p(t)$ constitute an attitude parameterization (Wertz, 1978). Estimation of p is based on the discrete-time, usually nonlinear, measurement equation:

$$b_{i,k+1} = D(p_{k+1})r_{i,k+1} + \delta b_{i,k+1} \quad (1)$$

where i identifies the sensor providing each vector measurement pair. Hence, $i=1$ tags the geomagnetic field vector, whereas $i=2$ is the unit vector pointing to the Sun. Index $k+1$ stands for discrete-time instant t_{k+1} . Measurement noise $\{\delta b_{i,k+1}\}$ is modeled as a zero mean, white sequence with covariance $R_{i,k+1}$.

Regarding the choice of attitude parameterization p , one recalls that the 3D rotation matrix given by a DCM $D(p)$ is in the orthonormal group $SO(3)$, and thus the dimension of p should be $n \geq 3$ (Stuelpnagel, 1964). The rotation quaternion $q(t) \in \mathfrak{R}^4$ is an attitude parameterization with the smallest dimension that is singularity-free, and its kinematics is described by a linear relationship (Lefferts *et al.*, 1982; Bar-Itzhack and Oschman, 1985). Thus, consider $q^T = [q_1 \ e^T]$ with q_1 and $e^T = [q_2 \ q_3 \ q_4]$ the scalar and vector representations, respectively, of the real and imaginary components of the rotation quaternion from S_r to S_b . The i -th vector measurement in equation (1) becomes:

$$b_{i,k+1} = D(q_{k+1})r_{i,k+1} + \delta b_{i,k+1} \quad D(q_{k+1}) = \begin{bmatrix} q_1^2 + q_2^2 - q_3^2 - q_4^2 & 2(q_2q_3 + q_1q_4) & 2(q_2q_4 - q_1q_3) \\ 2(q_2q_3 - q_1q_4) & q_1^2 - q_2^2 + q_3^2 - q_4^2 & 2(q_4q_3 + q_1q_2) \\ 2(q_2q_4 + q_1q_3) & 2(q_4q_3 - q_1q_2) & q_1^2 - q_2^2 - q_3^2 + q_4^2 \end{bmatrix}_{k+1} \quad (2)$$

The state equation for time propagation of the quaternion estimate of p between consecutive measurement data utilizes the attitude kinematics. The latter assumes distinct formulations that depend on the chosen attitude parameterization (Wertz, 1978). Its general formulation is given by the differential equation:

$$\dot{p} = f(p(t), \omega(t)) \quad (3)$$

and since the actual angular rate vector is unknown, one must provide an estimate of $\omega(t)$, as shall be seen later in this section. With the quaternion parameterization, the state equation becomes (Wertz, 1978):

$$\dot{q}(t) = \Omega(t) \cdot q(t) \quad \Omega(t) = \frac{1}{2} \begin{bmatrix} 0 & -\omega(t)^T \\ \omega(t) & -[\omega(t) \times] \end{bmatrix} \quad (4)$$

and $[\boldsymbol{\omega}(t) \times]$ is the outer product matrix with respect to angular rate vector $\boldsymbol{\omega}(t)$, which is represented in the S_b coordinate frame. One assumes $\boldsymbol{\omega}_k$ as the constant angular rate $\boldsymbol{\omega}(t)$ in the time interval $T = t_{k+1} - t_k$ between consecutive measurement data.

Joint estimation of attitude and angular rate estimation often employ the Euler equations, which describe angular rate changes and depend on knowledge of the satellite inertia and external torques. Therefore (Wertz, 1978):

$$\dot{\boldsymbol{\omega}}(t) = \mathbf{J}^{-1}[(\mathbf{J} \cdot \boldsymbol{\omega}(t)) \times \boldsymbol{\omega}(t)] + \mathbf{J}^{-1} \cdot \boldsymbol{\tau}(t) + \mathbf{w}(t) \quad (5)$$

and $\mathbf{J} \in \mathfrak{R}^{3 \times 3}$ is the inertia tensor, $\boldsymbol{\tau}(t) \in \mathfrak{R}^3$ is the known external control torque, and $\{\mathbf{w}(t) \in \mathfrak{R}^3\}$ is a white, zero-mean noise process approximating torque disturbances, and uncertainties in the inertia tensor and actuator model. $\boldsymbol{\tau}(t)$ is assumed constant between consecutive measurement data, that is, $\boldsymbol{\tau}(t) = \boldsymbol{\tau}_k \forall t \in [t_k, t_{k+1}]$. For joint estimation of attitude and angular rate, the augmented state is defined as the concatenation of the rotation quaternion and the angular rate, i.e., $\mathbf{x}^T = [q^T \boldsymbol{\omega}^T]$. The resulting nonlinear state dynamics is then:

$$\dot{\mathbf{x}} = \mathbf{f}(\mathbf{x}(t), \boldsymbol{\tau}(t)) + \mathbf{w}^d(t) \quad (6)$$

$$\mathbf{f}(\mathbf{x}, \boldsymbol{\tau}) = \begin{bmatrix} \boldsymbol{\Omega}(\boldsymbol{\omega}) \cdot \mathbf{q} \\ \mathbf{J}^{-1} \cdot [\mathbf{J} \cdot \boldsymbol{\omega} \times] \cdot \boldsymbol{\omega} + \mathbf{J}^{-1} \cdot \boldsymbol{\tau} \end{bmatrix} \quad (7)$$

with $[\mathbf{J} \cdot \boldsymbol{\omega} \times]$ denoting the outer product matrix with respect to the angular momentum vector $\mathbf{J} \cdot \boldsymbol{\omega}$. In equation (6), the model noise $(\mathbf{w}^d(t))^T = [\boldsymbol{\theta}_{1 \times 3}^T \mathbf{w}(t)^T]$, with $\{\mathbf{w}(t) \in \mathfrak{R}^3\}$ as defined in equation (5), is thus a white, zero-mean process with power spectral density \mathbf{Q} . Though the quaternion kinematics is deterministic, estimator implementation calls for tuning of \mathbf{Q} with all eigenvalues taking positive values, i.e., $\mathbf{Q} > \boldsymbol{\theta}$. This is aimed at maintaining the eigenvalues in the estimation error covariance matrix from converging to zero, and thus avoiding filter divergence. Recalling equation (2), the discrete-time measurement equation relating the vector measurement pairs of both the geomagnetic field $(\mathbf{b}_{1,k+1}, \mathbf{r}_{1,k+1})$ and the Sun sensor $(\mathbf{b}_{2,k+1}, \mathbf{r}_{2,k+1})$ to the augmented state is then:

$$\mathbf{b}_{k+1} = \mathbf{h}_{k+1}(\mathbf{x}_{k+1}) + \boldsymbol{\delta}\mathbf{b}_{k+1} \quad (8)$$

where

$$\mathbf{b}_{k+1} \triangleq \begin{bmatrix} \mathbf{b}_{1,k+1} \\ \mathbf{b}_{2,k+1} \end{bmatrix} \quad \mathbf{h}_{k+1}(\mathbf{x}_{k+1}) \triangleq \begin{bmatrix} \mathbf{D}(\mathbf{q}_{k+1}) \cdot \mathbf{r}_{1,k+1} \\ \mathbf{D}(\mathbf{q}_{k+1}) \cdot \mathbf{r}_{2,k+1} \end{bmatrix} \quad \boldsymbol{\delta}\mathbf{b}_{k+1} \triangleq \begin{bmatrix} \boldsymbol{\delta}\mathbf{b}_{1,k+1} \\ \boldsymbol{\delta}\mathbf{b}_{2,k+1} \end{bmatrix} \quad (9)$$

and where $\{\boldsymbol{\delta}\mathbf{b}_{1,k}\}$ and $\{\boldsymbol{\delta}\mathbf{b}_{2,k}\}$ are uncorrelated, white, zero-mean sequences with known covariances $\mathbf{R}_{1,k}$ and $\mathbf{R}_{2,k}$. Thus, $\boldsymbol{\delta}\mathbf{b}_k$ is a zero-mean, white sequence with covariance:

$$\mathbf{R}_k = \begin{bmatrix} \mathbf{R}_{1,k} & \mathbf{0}_{3 \times 3} \\ \mathbf{0}_{3 \times 3} & \mathbf{R}_{2,k} \end{bmatrix} \quad (10)$$

3. JOINT ATTITUDE AND ANGULAR RATE ESTIMATORS: AVEKF AND AVUKF

A continuous-discrete extended Kalman filter based on equations (6-7) and (8-10) is presented in Table 1. However, the linear update stage in the Kalman filter involves summing operations and does not ensure the unit magnitude of the estimated rotation quaternion. Generally, three approaches are used to deal with this condition: Euclidian, or “brute-force”, normalization after the update stage (Bar-Itzhack and Oshman, 1985), use of $q^T \cdot q = 1$ as a pseudo-measurement, which has not presented an acceptable convergence rate, and the more complex multiplicative approach (Lefferts *et al.*, 1982) based on the product of the quaternion error and the reference quaternion, with both having unit magnitude. Here, the Euclidian norm has been used and its effect on the corresponding estimation error is neglected as described in the analysis by Bar-Itzhack and Oshman (1985):

$$\hat{\mathbf{q}}_{k|k}^* = \hat{\mathbf{q}}_{k|k} / \|\hat{\mathbf{q}}_{k|k}\| \quad \text{and} \quad \mathbf{P}_{k+1|k+1}^* = \mathbf{P}_{k+1|k+1} \quad (11)$$

The EKF requires the state and measurement Jacobian matrices found in Appendix B of Santos (2008):

$$F(\hat{\mathbf{x}}(t), \boldsymbol{\tau}(t)) = \left. \frac{\partial \mathbf{f}(\mathbf{x}, \boldsymbol{\tau}(t))}{\partial \mathbf{x}} \right|_{\mathbf{x}=\hat{\mathbf{x}}(t)} \quad \text{and} \quad \mathbf{H}_{k+1} = \left. \frac{\partial \mathbf{h}_{k+1}(\mathbf{x})}{\partial \mathbf{x}} \right|_{\mathbf{x}=\hat{\mathbf{x}}_{k+1|k}} \quad (12)$$

Table 1. Attitude and angular velocity, extended Kalman filter – AVEKF.

Parameters	\mathbf{R}_k (Known data)	\mathbf{Q} (Tuned)
Initialization	$\hat{\mathbf{x}}_{00}^* = [\hat{\mathbf{q}}_0^T \hat{\boldsymbol{\omega}}_0^T]^T$	$\mathbf{P}_{00}^* = \mathbf{P}_0$
1a – State estimate propagation ^(a)	$\dot{\hat{\mathbf{x}}}(t) = \mathbf{f}(\hat{\mathbf{x}}(t), \boldsymbol{\tau}(t))$ $\dot{\mathbf{P}}(t) = \mathbf{F}(\hat{\mathbf{x}}(t), \boldsymbol{\tau}(t)) \cdot \mathbf{P}(t) + \mathbf{P}(t) \cdot \mathbf{F}(\hat{\mathbf{x}}(t), \boldsymbol{\tau}(t))^T + \mathbf{Q}$	
1b – Measurement prediction	$\hat{\mathbf{b}}_{k+1 k} = \mathbf{h}_{k+1}(\hat{\mathbf{x}}_{k+1 k})$ $\mathbf{P}_{k+1 k}^b = (\mathbf{H}_{k+1}) \cdot \mathbf{P}_{k+1 k} \cdot (\mathbf{H}_{k+1})^T + \mathbf{R}_{k+1}$	
1c – Cross covariance	$\mathbf{P}_{k+1 k}^{xb} = \mathbf{P}_{k+1 k} \cdot (\mathbf{H}_{k+1})^T$	
2a – Gain	$\mathbf{K}_{k+1} = \mathbf{P}_{k+1 k}^{xb} \cdot (\mathbf{P}_{k+1 k}^b)^{-1}$	
2b – State estimate update	$\hat{\mathbf{x}}_{k+1 k+1} = \hat{\mathbf{x}}_{k+1 k} + \mathbf{K}_{k+1} \cdot (\mathbf{b}_{k+1} - \hat{\mathbf{b}}_{k+1 k})$ $\mathbf{P}_{k+1 k+1} = \mathbf{P}_{k+1 k} - \mathbf{K}_{k+1} \cdot \mathbf{P}_{k+1 k}^b \cdot (\mathbf{K}_{k+1})^T$	
3 – Normalization	$\hat{\mathbf{q}} = [\hat{x}_1 \hat{x}_2 \hat{x}_3 \hat{x}_4]_{k+1 k+1}^T$ $\hat{\mathbf{x}}_{k+1 k+1}^* = [\hat{\mathbf{q}}^* \hat{x}_5 \hat{x}_6 \hat{x}_7]_{k+1 k+1}^T$	$\hat{\mathbf{q}}^* = \hat{\mathbf{q}} / \ \hat{\mathbf{q}}\ $ $\mathbf{P}_{k+1 k+1}^* = \mathbf{P}_{k+1 k+1}$
4 – Return to (1).		

(a) Numerical integration of differential equations in (1a) is accomplished with a fourth-order Runge-Kutta method with a fixed step of size $h=0.1s$ and proceeding from initial conditions $\hat{\mathbf{x}}_{k|k}$ and $\mathbf{P}_{k|k}$.

The unscented transformation (*TU*) approximates the mean and covariance of random variables undergoing a nonlinear transformation such as in equations (8-9). It has been proposed to steer away from difficulties in the extended Kalman filter arising due to linearization by means of truncation of the Taylor series (Julier and Uhlman, 2004). Instances of such difficulties are: 1) for the model to be reliable, the process being modeled should present quasi-linear dynamics; 2) the state dynamics and measurement functions, respectively \mathbf{f} and \mathbf{h} in equations (6) and (8), should be differentiable; and 3) the complex, and error-prone, derivation of the Jacobian matrices in equation (12). A description of the unscented transformation used in Santos (2008) and shown in Table 2 can be found in Julier and Uhlman (1997) and Sarkka (2007). The unscented integration (*IU*) is a similar approach dealing with the transformation of random processes by nonlinear stochastic differential equations such as in equations (6-7). A thorough discussion is found in Sarkka (2007) and revised for the present purpose of ITASAT attitude estimation in Santos (2008).

Table 2. Attitude and angular velocity, unscented Kalman filter – AVUKF.

Parameters	\mathbf{R}_k (Known data)	\mathbf{Q} (Tuned)
Initialization	$\hat{\mathbf{x}}_{00}^* = [\hat{\mathbf{q}}_0^T \hat{\boldsymbol{\omega}}_0^T]^T$	$\mathbf{P}_{00}^* = \mathbf{P}_0$
1a - State estimate propagation ^(a)	$[\hat{\mathbf{x}}_{k+1 k}, \mathbf{P}_{k+1 k}] = IU(\hat{\mathbf{x}}_{k k}, \mathbf{P}_{k k}, \mathbf{f}(\cdot, \boldsymbol{\tau}(t)), \mathbf{Q})$	
1b – Measurement prediction	$[\hat{\mathbf{b}}_{k+1 k}, \bar{\mathbf{P}}_{k+1 k}^b, \mathbf{P}_{k+1 k}^{xb}] = TU(\hat{\mathbf{x}}_{k+1 k}, \mathbf{P}_{k+1 k}, \mathbf{h}_{k+1}(\cdot))$ $\mathbf{P}_{k+1 k}^b = \bar{\mathbf{P}}_{k+1 k}^b + \mathbf{R}_{k+1}$	
2a – Gain	$\mathbf{K}_{k+1} = \mathbf{P}_{k+1 k}^{xb} \cdot (\mathbf{P}_{k+1 k}^b)^{-1}$	
2b – State estimate update	$\hat{\mathbf{x}}_{k+1 k+1} = \hat{\mathbf{x}}_{k+1 k} + \mathbf{K}_{k+1} \cdot (\mathbf{b}_{k+1} - \hat{\mathbf{b}}_{k+1 k})$ $\mathbf{P}_{k+1 k+1} = \mathbf{P}_{k+1 k} - \mathbf{K}_{k+1} \cdot \mathbf{P}_{k+1 k}^b \cdot (\mathbf{K}_{k+1})^T$	
3 – Normalization	$\hat{\mathbf{q}} = [\hat{x}_1 \hat{x}_2 \hat{x}_3 \hat{x}_4]_{k+1 k+1}^T$ $\hat{\mathbf{x}}_{k+1 k+1}^* = [\hat{\mathbf{q}}^* \hat{x}_5 \hat{x}_6 \hat{x}_7]_{k+1 k+1}^T$	$\hat{\mathbf{q}}^* = \hat{\mathbf{q}} / \ \hat{\mathbf{q}}\ $ $\mathbf{P}_{k+1 k+1}^* = \mathbf{P}_{k+1 k+1}$
4 – Return to (1).		

(a) Numerical integration of differential equations in (1a) is accomplished with a fourth-order Runge-Kutta method with a fixed step of size $h=0.1s$ and proceeding from initial conditions $\hat{\mathbf{x}}_{k|k}^*$ and $\mathbf{P}_{k|k}^*$.

4. MAGNETOMETER BIAS ESTIMATION

The accuracy of magnetometer-based attitude estimation is strongly affected by calibration (Crassidis *et al.*, 2005). Pre-flight bias, scale factor, and non-orthogonality are estimated in lab conditions. However, significant changes may

occur after satellite launch. Scale factor and non-orthogonality are affected by thermal gradients and mechanical stress. Bias variations are due to changes in the satellite's residual magnetic field and magnetic interferences in the vicinity of the magnetometer. The TWOSTEP algorithm (Alonso and Shuster, 2002a) estimates magnetometer bias without need for any knowledge about attitude. The algorithm has been extended to estimate scale factor and non-orthogonality (Alonso and Shuster, 2002b). Based on this extension, Crassidis *et al.* (2005) formulated recursive estimators, EKF and unscented KF, for real-time magnetometer calibration. Here, only bias calibration is focused via estimation with TWOSTEP providing the measurement equation. The bias state is $\mathbf{c}^T = [c_x, c_y, c_z]$, which is considered a discrete-time Wiener process:

$$\mathbf{c}_{k+1} = \mathbf{c}_k + \delta\mathbf{c}_k \quad (13)$$

and $\{\delta\mathbf{c}_k\}$ is a white, zero mean sequence with covariance \mathbf{Q}^c . Assume the magnetometer with unit scale factors and perfectly orthogonal axes. Then the raw measurement $\tilde{\mathbf{b}}_{l,k}$ at instant t_k is modeled as:

$$\tilde{\mathbf{b}}_{l,k} = \mathbf{D}_k \cdot \mathbf{r}_{l,k} + \mathbf{c}_k + \delta\mathbf{b}_{l,k} \quad (14)$$

where \mathbf{D}_k is the DCM from S_r to the magnetometer coordinate frame $S_m \equiv \{X_m, Y_m, Z_m\}$, \mathbf{c}_k is the bias vector, and $\{\delta\mathbf{b}_{l,k}\}$ is a white sequence with zero mean and covariance $\mathbf{R}_{l,k}$. The scalar measurement model is as described by Alonso and Shuster (2002a):

$$z_{k+1} = h_{k+1}^c(\mathbf{c}_{k+1}) + \delta z_{k+1} \quad (15)$$

where

$$z_{k+1} \Delta \|\tilde{\mathbf{b}}_{1,k+1}\| - \|\mathbf{r}_{1,k+1}\| \quad \text{and} \quad h_{k+1}^c(\mathbf{c}_{k+1}) \Delta 2 \cdot \tilde{\mathbf{b}}_{1,k+1}^T \cdot \mathbf{c}_{k+1} - \mathbf{c}_{k+1}^T \cdot \mathbf{c}_{k+1}$$

and $\{\delta z_{k+1}\}$ is a Gaussian, white sequence with mean and covariance, respectively, given by:

$$\mu_{k+1} = -\text{trace}\{\mathbf{R}_{1,k+1}\} \quad (16)$$

$$\sigma_{k+1}^2 = 4 \cdot (\tilde{\mathbf{b}}_{1,k+1} - \mathbf{c}_{k+1})^T \cdot \mathbf{R}_{1,k+1} \cdot (\tilde{\mathbf{b}}_{1,k+1} - \mathbf{c}_{k+1}) + 2 \cdot \text{trace}\{\mathbf{R}_{1,k+1}^2\} \quad (17)$$

Variance σ_{k+1}^2 depends on the bias ground-truth \mathbf{c}_{k+1} . However, given its unknown value, the estimator has used $\hat{\mathbf{c}}_{k+1/k}$ instead. In such a case, the measurement noise variance in the filter is the estimate $\hat{\sigma}_{k+1}^2$. Moreover, the nonzero mean of measurement noise sequence $\{\delta z_{k+1}\}$ must be considered in the predicted measurement in the bias estimator. Tables 3 and 4 display the magnetometer bias estimators: MAGEKF and MAGUKF, based on extended and unscented Kalman filtering, respectively, and use of state and measurement equations (16) and (18), correspondingly. The measurement Jacobian $\mathbf{H}_{k+1}^c = \partial h_{k+1}^c(\mathbf{c}) / \partial \mathbf{c}$ at $\mathbf{c} = \hat{\mathbf{c}}_{k+1/k}$ in MAGEKF is in Appendix B of Santos (2008).

Table 3. Magnetometer bias extended Kalman filter – MAGEKF.

Parameters	$\mathbf{R}_{1,k}$ (Known)	\mathbf{Q}^c (Tuned)
Initialization	$\hat{\mathbf{c}}_{00} = \hat{\mathbf{c}}_0$	$\mathbf{P}_{0 0} = \mathbf{P}_0^c$
1a – State estimate propagation	$\hat{\mathbf{c}}_{k+1 k} = \hat{\mathbf{c}}_{k k}$ $\mathbf{P}_{k+1 k} = \mathbf{P}_{k k} + \mathbf{Q}^c$	
1b – Measurement prediction	$\hat{z}_{k+1 k} = h_{k+1}^c(\hat{\mathbf{c}}_{k+1 k}) + \mu_{k+1}$ $\mathbf{P}_{k+1 k}^z = (\mathbf{H}_{k+1}^c) \cdot \mathbf{P}_{k+1 k} \cdot (\mathbf{H}_{k+1}^c)^T + \hat{\sigma}_{k+1}^2$	
1c – Cross covariance	$\mathbf{P}_{k+1 k}^{cz} = \mathbf{P}_{k+1 k} \cdot (\mathbf{H}_{k+1}^c)^T$	
2a – Gain	$\mathbf{K}_{k+1} = \mathbf{P}_{k+1 k}^{cz} \cdot (\mathbf{P}_{k+1 k}^z)^{-1}$	
2b – State estimate update	$\hat{\mathbf{c}}_{k+1 k+1} = \hat{\mathbf{c}}_{k+1 k} + \mathbf{K}_{k+1} \cdot (z_{k+1} - \hat{z}_{k+1 k})$ $\mathbf{P}_{k+1 k+1} = \mathbf{P}_{k+1 k} - \mathbf{K}_{k+1} \cdot \mathbf{P}_{k+1 k}^z \cdot \mathbf{K}_{k+1}^T$	
3 – Return to (1).		

Table 4. Magnetometer bias extended Kalman filter – MAGUKF.

Parameters	$\mathbf{R}_{1,k}$ (Known)	\mathbf{Q}^c (Tuned)
Initialization	$\hat{\mathbf{c}}_{00} = \hat{\mathbf{c}}_0$	$\mathbf{P}_{0,0} = \mathbf{P}_0^c$
1a - State estimate propagation	$\hat{\mathbf{c}}_{k+1 k} = \hat{\mathbf{c}}_{k k}$ $\mathbf{P}_{k+1 k} = \mathbf{P}_{k k} + \mathbf{Q}^c$	
1b – Measurement prediction	$[\bar{\mathbf{z}}_{k+1 k}, \bar{\mathbf{P}}_{k+1 k}^z, \mathbf{P}_{k+1 k}^{cz}] = \text{TU}(\hat{\mathbf{c}}_{k+1 k}, \mathbf{P}_{k+1 k}, \mathbf{h}_{k+1}^c(\cdot))$ $\hat{\mathbf{z}}_{k+1 k} = \bar{\mathbf{z}}_{k+1 k} + \boldsymbol{\mu}_{k+1}$ $\mathbf{P}_{k+1 k}^z = \bar{\mathbf{P}}_{k+1 k}^z + \hat{\boldsymbol{\sigma}}_{k+1}^2$	
2a – Gain	$\mathbf{K}_{k+1} = \mathbf{P}_{k+1 k}^{cz} \cdot (\mathbf{P}_{k+1 k}^z)^{-1}$	
2b – State estimate update	$\hat{\mathbf{c}}_{k+1 k+1} = \hat{\mathbf{c}}_{k+1 k} + \mathbf{K}_{k+1} \cdot (\mathbf{z}_{k+1} - \hat{\mathbf{z}}_{k+1 k})$ $\mathbf{P}_{k+1 k+1} = \mathbf{P}_{k+1 k} - \mathbf{K}_{k+1} \cdot \mathbf{P}_{k+1 k}^z \cdot \mathbf{K}_{k+1}^T$	
3 – Return to (1).		

5. ITASAT'S ATTITUDE DETERMINATION SYSTEM (SDA)

Figure 2 shows the proposed SDA for ITASAT. Its components are briefly described in the following.

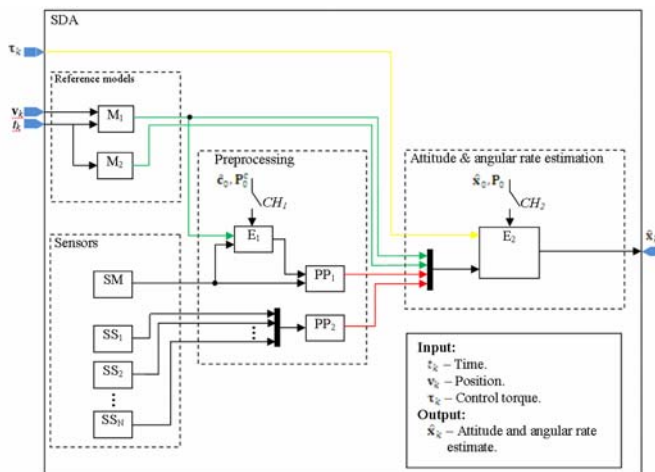


Figure 2. SDA for low-cost ITASAT satellite.

The geomagnetic field model M_1 is WMM2005 (McLean *et al.*, 2004). It consists of a series expansion of spherical harmonics up to the 12-th degree, and provides the reference geomagnetic field measurement vector in the set $\mathbf{R}(t) = \{r_i(t) \in \mathfrak{R}^3, i = 1, 2, \dots, m\}$ seen in Section 2. The M_1 model requires knowledge of sensor time tag t_k at the sampling instants, and satellite position \mathbf{v}_k . Concurrently, algorithm 29 in Vallado (2004) provides the reference model M_2 that yields the reference Sun direction measurement vector in the aforementioned set.

A 3D magnetometer (SM) and Sun sensors ($SS_n, n=1, \dots, 3$) are onboard ITASAT. Three Sun sensors located as in Figure 1 with a full-hemisphere field-of-view ensure a line of sight to the Sun, except during an eclipsed. Magnetometer output is the measured geomagnetic field in the magnetometer coordinate frame S_m . Each Sun sensor provides a pair of angles ϕ and θ to compute the unit vector pointing to the Sun in the body coordinate frame S_b . All sensor are assumed to provide data at the same time tag t_k .

Preprocessing aims at providing the vector measurements in body coordinate frame representation. Assuming to be known the magnetometer with unit scale factor and the DCM \mathbf{D}_m^b of sensor coordinate frame S_m attitude relative to S_b , then block $PP1$ in Figure 2 computes vector measurement \mathbf{b}_1 from raw measurement $\tilde{\mathbf{b}}_1$ as follows:

$$\mathbf{b}_1 = (\mathbf{D}_m^b)^T \cdot (\tilde{\mathbf{b}}_1 - \hat{\mathbf{c}}) \quad (18)$$

and \hat{c} is the magnetometer bias estimate output by E_I . The estimator in E_I can be either MAGEKF or MAGUKF, and is initialized with \hat{c}_0 and \mathbf{P}_0^c by closing switch CH_I . This switching should occur previous attitude and angular rate estimation to provide sufficient time for the convergence of the magnetometer bias estimator.

Preprocessing of Sun sensor measurements in $PP2$ is carried out in three stages. First of all is the selection of the Sun sensor whose normal direction is nearest to the unit vector pointing to the Sun. Secondly, once chosen SS_j as the most appropriate Sun sensor, the unit vector pointing to the Sun \mathbf{s}_j is computed from measured elevation and azimuth angles, respectively ϕ_j and θ_j , in the j -th Sun sensor coordinate frame S_{sj} . Thirdly, since DCM \mathbf{D}_j^b is given, representation of $\mathbf{s}_j^T = [\cos(\phi_j).\sin(\theta_j) \quad \cos(\phi_j).\cos(\theta_j) \quad \sin(\phi_j)]$ in S_b is obtained according to:

$$\mathbf{b}_2 = (\mathbf{D}_j^b)^T \cdot \mathbf{s}_j \quad (19)$$

The estimator in block E_2 , either AVEKF or AVUKF, is initialized with $\hat{\mathbf{x}}_0$ and \mathbf{P}_0 when switch CH_2 is closed. This estimator requires as input the preprocessed measurement vectors – geomagnetic field \mathbf{b}_1 , and unit vector pointing to the Sun \mathbf{b}_2 – and the control torque $\boldsymbol{\tau}$ produced by the attitude control system ACS, which is assumed to be known.

6. SIMULATION AND RESULTS

The Attitude Determination System (SDA) has been tested by Monte Carlo simulation with synthetic measurement data. Section 6.1 focuses on magnetometer bias estimation, and Section 6.2 on attitude and angular rate estimation. Control torque $\boldsymbol{\tau}$ is assumed null without incurring in loss of applicability. Epoch is January 01 2008 12:00:00 GMT. Keplerian elements are used for nominal orbit specification: 7,128km semi-major axis, 0.001 eccentricity, 25° inclination, -40° right ascension of the ascending node, 12° argument of perigee, 0 perigee passage time. Torque disturbances taken into consideration are due to: 1) gravity gradient; 2) residual magnetic dipole moment $\mathbf{m}=[0.1 \quad 0.1 \quad 0.1]^T A.m^2$; and 3) a zero-mean Gaussian torque with covariance $(1.0 \times 10^{-12}).\mathbf{I}_3 (N.m)^2$. Wertz (1978) provides models for torque disturbances caused by gravity gradient and residual magnetism. True inertia tensor in S_b coordinates is $\mathbf{J}^b=diag(6.5 \quad 6.5 \quad 8.0)kg.m^2$. Angular rate and attitude motion equations are solved numerically with fourth-order Runge-Kutta and a 0.001s step size. Further details are in Santos (2008). Synthesis of geomagnetic field measurements are based on WMM2005 and making use of various coordinate transformations (Vallado,2004).

For the sake of simplification, both the magnetometer and the sole Sun sensor considered in the simulation have coordinate frames in alignment with S_b . Actual magnetometer error $\delta\mathbf{b}_{1,k}$ consists of component-wise Markov-Gaussian sequences with $T_m=100s$ correlation time driven by a zero-mean, white sequence with covariance $q_m.\mathbf{I}_3$, with $q_m=1.0 \times 10^{-11}(T)^2$ (Shorshi and Bar-Itzhack, 1995) in addition to a zero-mean, white sequence with covariance $\mathbf{R}_{1,k}=4.0 \times 10^{-14}.\mathbf{I}_3 (T)^2$. Actual Sun angle measurement error $\{\delta\phi_{s,k} \quad \delta\theta_{s,k}\}^T$ is a zero-mean Gaussian sequence with covariance $\mathbf{R}_{\phi\theta}=(0.5.\pi/180)^2.\mathbf{I}_2 rad^2$. Figure 3 depicts the angle sequence from sensor frame to Sun direction: azimuth $\theta_{s,k}$ first, followed by elevation $\phi_{s,k}$.

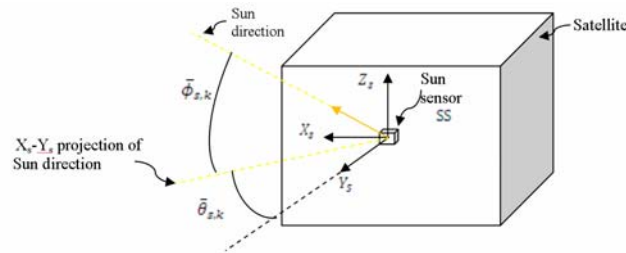


Figure 3. Sun sensor error-free angles.

The relevant vector measurements for filter operation are then synthesized as:

$$\mathbf{b}_{1,k} = \mathbf{D}_b^f(\mathbf{q})\mathbf{r}_{1,k} + \delta\mathbf{b}_{1,k} = \bar{\mathbf{b}}_{1,k} + \delta\mathbf{b}_{1,k} \quad (20)$$

$$\mathbf{b}_{2,k} = \mathbf{D}_b^f(\mathbf{q})\mathbf{r}_{2,k} + \delta\mathbf{b}_{2,k} = \bar{\mathbf{b}}_{2,k} + \delta\mathbf{b}_{2,k} \quad (21)$$

The estimators require the statistics of the error $\delta\mathbf{b}_{2,k}$ in the Sun-pointing unit vector $\mathbf{b}_{2,k}$, which relate to Sun angular measurement errors due to:

$$\delta \mathbf{b}_{2,k} \approx \mathbf{\Pi}_k \cdot \begin{bmatrix} \delta \phi_{s,k} \\ \delta \theta_{s,k} \end{bmatrix} \mathbf{\Pi}_k \Delta \begin{bmatrix} -\sin(\phi_{s,k}) \cdot \sin(\theta_{s,k}) & \cos(\phi_{s,k}) \cdot \cos(\theta_{s,k}) \\ -\sin(\phi_{s,k}) \cdot \cos(\theta_{s,k}) & -\cos(\phi_{s,k}) \cdot \sin(\theta_{s,k}) \\ \cos(\phi_{s,k}) & 0 \end{bmatrix} \quad (22)$$

Because the covariance of angle error $\mathbf{R}_{\phi\theta}$ has rank 2, the covariance $\mathbf{R}_{2,k} = \mathbf{\Pi}_k \cdot \mathbf{R}_{\phi\theta} \cdot \mathbf{\Pi}_k^T \in \mathfrak{R}^{3 \times 3}$ of error $\delta \mathbf{b}_{2,k}$ for use in the estimator yields a singular matrix that may lead to filter divergence. This is avoided by use of the approximated covariance $\mathbf{R}_{2,k} \cong \mathbf{\Pi}_k \cdot \mathbf{R}_{\phi\theta} \cdot \mathbf{\Pi}_k^T + \beta \cdot \mathbf{I}_3$ in the filter with $\beta = 1.0 \times 10^{-6}$.

Three distinct motions have been considered for evaluating estimator performance. The slow motion is initialized with the satellite rotating at approximately 1 rotation per orbit about the major inertia axis, Z_b , which is perpendicular to the ecliptic. The spin motion consists of a 40rpm rate about the spin axis Z_b , and included nutation caused by slower angular rates about the other orthogonal, principal axes. Finally, tumbling mimics a condition likely to occur when the satellite is injected into orbit by a 3-axis controlled last stage of a launch vehicle. Santos(2008) details the respective initial conditions.

Regarding ground-truth satellite position \mathbf{v}_k , it is generated by the satellite motion along its nominal orbit and disturbed by additive zero-mean white Gaussian sequence with covariance $100 \cdot \mathbf{I}_3 (\text{km})^2$. Actual time tag t_k is the same as that used in the SDA estimator.

6.1 Magnetometer bias estimation

Ground-truth magnetometer bias is $\mathbf{c} = [5.0 \ 5.0 \ 5.0]^T \cdot 10^{-6} T$ and both the MAGEKF and MAGUKF estimators have been initialized with $\hat{\mathbf{c}}_0 \sim N(\mathbf{0}_{3 \times 1}, \sigma_c^2 \cdot \mathbf{I}_3)$ and $\mathbf{P}_0^c = \sigma_c^2 \cdot \mathbf{I}_3$ and $\sigma_c = 1.0 \times 10^{-5} T$. State covariance noise has been tuned to $\mathbf{Q}^c = 1.0 \times 10^{-12} \cdot \mathbf{I}_3 (T)^2$. A Monte Carlo simulation has been carried out to yield 100 realizations of the bias estimate at the final time t_f for each of the slow, spinning, and tumbling motions. The selected 1-hour data window initiated at 12:00:00 GMT of January 01 2008 with a 1s sampling time has been used for the spinning and tumbling motions. Regarding the slow motion, 1-hour data windows were not sufficient for the bias estimators to converge. In this case, an 8-hour window was utilized with a 10s sampling time. MAGUKF estimates at t_f presented a slightly larger standard deviation in all motion conditions, but always kept under 0.2mG. Component-wise estimation errors in all cases were below $2.0 \times 10^{-7} T$ though (1mG = $10^{-7} T$). Furthermore, the MAGUKF execution time was about twice that of the MAGEKF. Details are found in Santos(2008).

6.2 Joint attitude and angular rate estimation

From the previous subsection, an instance of the residual bias given by $\mathbf{c}_{res} = [-2 \ -2 \ -2]^T \cdot 10^{-7} T$ has been considered in magnetometer measurements. Other instances, obtained by distinct permutations of the above component-wise values, have not changed the results in a significant way. The data window was 1,000s long at epoch 20:00:00 GMT January 1 2008. Eclipse occurrences were disregarded at this stage, that is, direct line of sight to the Sun was assumed at all times. The TRIAD static approach has been employed to yield an initial estimate of the attitude as described in page 424 of Wertz (1978). The initial estimate of the angular rate has been modeled as a zero-mean, Gaussian random variable with covariance $\sigma_0^2 \cdot \mathbf{I}_3$, where $\sigma_0 = 10 \cdot \pi / 180 \text{ rad/s}$, in addition to the ground-truth value. Diagonal state noise power spectral density \mathbf{Q} has been tuned by means of estimator performance evaluation (Santos, 2008), as well as the joint estimator's initial state covariance matrix \mathbf{P}_0 . Sun direction measurement error covariance $\mathbf{R}_{2,k}$ has been computed from Sun angle measurement error covariance $\mathbf{R}_{\phi\theta}$ as in equation (22) and the corresponding clarifications in the accompanying text.

Parameter κ in the unscented transformation (TU) and unscented integration (IU) has been selected according to the rule $\kappa = 3 - n$ where n is the state vector dimension (Julier and Uhlman, 1997, 2004; Sarkka, 2007). The inertia tensor used by both AVEKF and AVUKF is:

$$\mathbf{J} = \begin{bmatrix} 6.508 & 0.008 & -0.008 \\ 0.008 & 6.492 & -0.008 \\ -0.008 & -0.008 & 8.008 \end{bmatrix} \text{kg.m}^2 \quad (23)$$

Errors with a magnitude of 0.1% of the maximum inertia ground-truth value $\mathbf{J}_{33}^* = 8.0 \text{kg.m}^2$ have been added to the ground-truth values in \mathbf{J} . Element signs in the inertia tensor have been assigned arbitrarily after simulations showed that results have not changed significantly in terms of attitude and angular rate estimation accuracy. Sensor sampling time is $T = 0.1 \text{s}$. Attitude and angular rate estimation error performance at the k -th time step has been evaluated from the sample averages \bar{I}_k and \bar{F}_k and corresponding standard deviations σ_k^I and σ_k^F of 100 realizations of the following random variables, respectively I_k and F_k :

$$I_k = \left| \text{acos}\left(\frac{1}{2} \text{trace}(\mathbf{D}(\hat{\mathbf{p}}_{k|k})^T \cdot \mathbf{D}(\hat{\mathbf{p}}_k)) - \frac{1}{2}\right) \right| \quad (30)$$

$$F_k = \left[(\hat{\boldsymbol{\omega}}_{k|k} - \boldsymbol{\omega}_k)^T \cdot (\hat{\boldsymbol{\omega}}_{k|k} - \boldsymbol{\omega}_k) \right]^{1/2} \quad (31)$$

Notice that attitude estimation error index I_k has been defined as the magnitude of the rotation angle about the rotation axis between the ground-truth satellite attitude and its estimate. There were no significant differences between AVEKF and AVUKF in terms of estimation accuracy and convergence rate. For all motions involved in the analysis, steady-state attitude estimation error statistics remained at about 1 degree. For lack of space, figures with the results are found in Santos (2008). Peak values of $\bar{I}_k + 3 \times \sigma_k^I$ and $\bar{F}_k + 3 \times \sigma_k^F \quad \forall t_k \in (100, 1,000][s]$ for distinct sensor sampling time values $T = \{0.1; 0.5; 1.0\}[s]$ were considered. Both attitude and angular rate estimation accuracy degraded as sampling time T increased. AVEKF estimates have suffered slightly earlier than AVUKF's with the raising of T values. Worst-case attitude estimation error $\bar{I}_k + 3 \times \sigma_k^I$ remained under 2.06 degrees when tumbling with $T=1.0s$ whereas the worst angular rate index $\bar{F}_k + 3 \times \sigma_k^F$ has not exceeded 5 degrees/s when spinning at 40rpm with $T=1.0s$, and stayed below 0.2 degree/s when tumbling and 0.02 degree/s when subject to slow motion. The computational load of the AVUKF has been roughly three times heavier than that of the AVEKF.

ITASAT's target orbit parameters are such that eclipse intervals shall occur during approximately 35% of the orbit period. Magnetometer readings then become the only vector measurement available for attitude determination. Tests under eclipse conditions have been conducted with both the AVEKF and AVUKF with a 6,000s data window, which is approximately one orbit, at epoch 20:00:00 GMT January 1 2008. The eclipse interval spanned from 1,000s up to 3,110s, and sampling time was $T=0.1s$. Estimation during tumbling was not significantly altered by the eclipse and is not shown here for lack of space. Figure 7 shows statistics resulting from 10 realizations. Blue depicts \bar{I}_k or \bar{F}_k , whereas red represents $\bar{I}_k + 3 \times \sigma_k^I$ or $\bar{F}_k + 3 \times \sigma_k^F$.

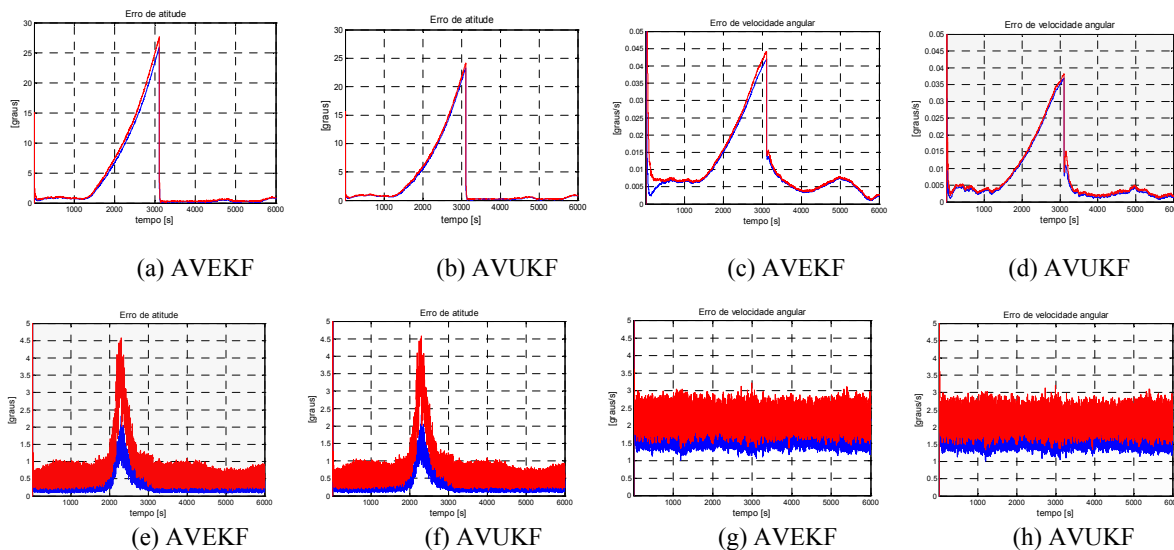


Figure 7 Attitude and angular rate estimation accuracy during one orbit with eclipse – slow motion: (a-b) attitude estimation error, (c-d) angular rate estimation error – spinning motion: (e-f) attitude error, and (g-h) angular rate estimation error.

With respect to Figure 7, (c-d) indicate that a minor angular rate estimation divergence during the eclipse occurred when undergoing slow motion. On the other hand, (g-h) show that the angular rate estimation degradation is practically imperceptible when the satellite is undergoing spinning motion because of the high angular momentum.

Recall that errors in angular rate estimation accumulate and couple with attitude kinematics in both AVEKF and AVUKF, thus yielding the attitude estimation errors seen in Figure 7. In the case of slow motion shown in (a-b), attitude estimates diverge and reach a peak of about 25 degrees by the end of the eclipse interval. Fortunately, adequate attitude estimation accuracy is rapidly recovered soon after the end of the eclipse. Concerning the smaller attitude estimation peak error during eclipse while subject to spinning shown in (e-f) at about 2,200s, Figure 8 shows the extreme reduction in geomagnetic field measurements along the satellite spin plane directions X_b and Y_b in the vicinity of 2,200s. The

falling signal-to-noise ratio between the geomagnetic ground-truth and magnetometer noise along those spin plane directions caused the degradation of the attitude estimates about spin axis Z_b .

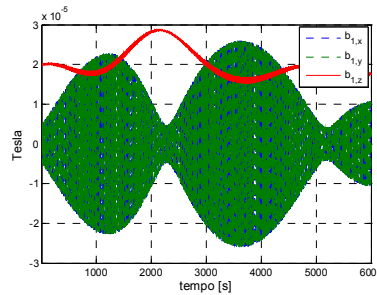


Figure 8. Geomagnetic field measurements during spinning motion

7. CONCLUSION

The performance of two joint estimators of low-cost ITASAT attitude and angular rate, the AVEKF and the AVUKF, were investigated with the aiding of magnetometer bias estimators MAGEKF and MAGUKF for improved results. The accuracy attained from Monte Carlo statistics, though crude as it remained in steady-state in about two degrees in the worst case when tumbling with $T=1.0s$, adhered to ITASAT's attitude control specification when the Sun is visible. Differently from the previous SCD satellite series equipped with nutation damping rings partially filled with silicone oil, here angular rate estimation is called for to carry out active nutation damping with adequate magnetotorquers activation. ITASAT's 3-axis estimation-based attitude control prior to acquiring spin stabilization has been devised to cope with the likelihood of initial slow motion in case of injection into orbit by a 3-axis controlled launcher. Recent results have shown the efficacy of magnetotorquer-only actuation for nutation angle attenuation (Waschburger *et al.*, 2008a, 2008b), thus avoiding the complicated modeling of the sloshing disturbances in a nutation damping ring subject to slow motion.

The attitude errors indicate that closed-loop attitude control may be unfeasible during eclipse intervals, if the satellite is to undergo slow motion. Hence, if such launch condition occurs, it is strongly recommended that, given ITASAT's thermal safety constraints, attitude and angular rate estimates should be used for control solely when the Sun is visible to the satellite. Obviously, such consideration anticipates crucial implications concerning the definition of the satellite's *modus operandi* and the onboard battery capacity. Thus, ITASAT will take longer since separating from the launcher up to the onset of the operational phase with spin stabilization normal to the ecliptic plane and battery recharge. A tradeoff might involve reconsidering the target orbit. However, the latter is launcher-dependent: low-cost ITASAT is not expected to have its own, paid-for, launch mission. ITASAT is supposed to ride piggyback onto an available, possibly third-party, main payload. ITASAT's mission analysis team must be aware of the capabilities and limitations of the available attitude control, *vis-à-vis* the knowledge that, by the end of the day, ITASAT's target orbit is eventually going to be determined by that of an available launcher and the target orbit of its main payload.

8. ACKNOWLEDGEMENTS

This work was supported by project FINEP/FUNDEP/INPE/CTA 'SIA – Inertial Systems for Aerospace Application', and project AEB/INPE/CTA 'ITASAT – University Satellite'.

9. REFERENCES

- Alonso, R.; Shuster, M. D., 2002a, "TWOSTEP: A Fast Robust Algorithm for Attitude-Independent Magnetometer Bias Determination", The Journal of the Astronautical Sciences, Vol. 50, No. 4, pp. 433-451.
- Alonso, R.; Shuster, M. D., 2002b, "Complete Linear Attitude-Independent Magnetometer Calibration", The Journal of the Astronautical Sciences, Vol. 50, No. 4, pp. 477-490.
- Bak, T.; Wisniewski, R.; Blanke, M., 1996, "Autonomous Attitude Determination and Control System for the Orsted Satellite", IEEE Proceedings on Aerospace Applications Conference, Vol. 2, pp. 173-186.
- Bar-Itzhack, I. Y.; Oshman, Y., 1985, "Attitude Determination from Vector Observations: Quaternion Estimation", IEEE Transactions on Aerospace and Electronic Systems, Vol. AES-21, No. 1, pp. 128-135.
- Challa, M.; Natanson, G.; Wheeler, C., 1996, "Simultaneous Determination of Spacecraft Attitude and Rates Using Only a Magnetometer", AIAA/AAS Astrodynamics Conference, San Diego, CA.
- Crassidis, J. L.; Lai, K.-L.; Harman, R. R., 2005, "Real-Time Attitude-Independent Three-Axis Magnetometer Calibration", Journal of Guidance, Control, and Dynamics, Vol. 28, No. 1, pp. 115-120.
- Julier, S. J.; Uhlmann, J. K., 2004, "Unscented Filtering and Nonlinear Estimation", Proceedings of the IEEE, Vol. 92, No. 3, pp. 401-421.

- Julier, S. J.; Uhlmann, J. K., 1997, "A New Extension of the Kalman Filter to Nonlinear Systems", Proc. AeroSense: 11th International Symposium on Aerospace/Defense Sensing, Simulation and Controls, pp. 182-193.
- Krogh, K., 2002, "Attitude Determination for AAU CubeSat", M.Sc. thesis – Aalborg University, Aalborg.
- Lefferts, E. J.; Markley, F. L.; Shuster, M. D., 1982, "Kalman Filtering for Spacecraft Attitude Estimation", Journal of Guidance, Control, and Dynamics, Vol. 5, No. 5, pp. 417-429.
- Lopes, R.V. da F.; Ricci, M.C. and Guedes, U.T.V., 1986, "Partially Filled Viscous Ring Nutation Damper: Brief Description and Preliminary Design", INPE Technical Report NTI-AMNUT-007-DMC/86.
- McLean, S. S.; Macmillan, S.; Maus, V.; Lesur, A.; Thomson, D.; Dater, D., 2004, "The US/UK World Magnetic Model for 2005-2010", NOAA Technical Report NESDIS/NGDC-1.
- Santos, D.A., 2008, "Satellite attitude and angular rate estimation from Vector Measurements of the Geomagnetic Field and Sun Direction", M.Sc. Thesis – Instituto Tecnológico de Aeronáutica, Brazil (in Portuguese).
- Sarkka, S., 2007, "On Unscented Kalman Filtering for State Estimation of Continuous-Time Nonlinear Systems", IEEE Transactions on Automatic Control, Vol. 52, No. 9, pp. 1631-1641.
- Svartveit, K., 2003, "Attitude determination of the NCUBE satellite", M.Sc. thesis – NTNU, Trondheim.
- Shigehara, M., 1972, "Geomagnetic Attitude Control of an Axisymmetric Spinning Satellite", Journal of Spacecraft, v.9, no.6, pp. 391-398.
- Shorshi, G.; Bar-Itzhack, I. Y., 1995, "Satellite Autonomous Navigation Based on Magnetic Field Measurements", Journal of Guidance, Control, and Dynamics, Vol. 18, No. 4, pp. 843-850.
- Stuelpnagel, J., 1964, "On the Parameterization of the Three-Dimensional Rotation Group", SIAM Reviews, Vol. 6, No. 4, pp. 422-430.
- Vallado, D. A., 2004, "Fundamentals of Astrodynamics and Applications", Space Technology Library, 2nd ed.
- Wahba, G., 1965, "A Least-Squares Estimate of Satellite Attitude", SIAM Reviews, Vol. 7, No. 3, p. 409.
- Waschburger, R ; Viana, I. B. ; Nepomuceno, A. L. ; Waldmann, J., 2008a, "Simulation of University Satellite ITASAT for Feasibility Evaluation of Purely Magnetic Actuation", V Congresso Nacional de Engenharia Mecânica, Brazil (in Portuguese).
- Waschburger, R., Waldmann, J., 2008b, "Magnetotorquers Activation Criteria in University Satellite ITASAT's Attitude Control System with Purely Magnetic Actuation", Congresso Brasileiro de Automação, Brazil (in Portuguese).
- Wertz, J. (ed.), 1978, "Spacecraft Attitude Determination and Control", The Netherlands, Kluwer Academic Publishers.

10. RESPONSIBILITY NOTICE

The authors are the only responsible for the printed material included in this paper.